isvr Institute of Sound and Vibration Research

Wheel/Rail Non-Linear Interaction with Coupling between Vertical and Lateral Directions

T.X. Wu and D.J. Thompson

ISVR Technical Memorandum No 891

August 2002

University of Southampton

SCIENTIFIC PUBLICATIONS BY THE ISVR

Technical Reports are published to promote timely dissemination of research results by ISVR personnel. This medium permits more detailed presentation than is usually acceptable for scientific journals. Responsibility for both the content and any opinions expressed rests entirely with the author(s).

Technical Memoranda are produced to enable the early or preliminary release of information by ISVR personnel where such release is deemed to the appropriate. Information contained in these memoranda may be incomplete, or form part of a continuing programme; this should be borne in mind when using or quoting from these documents.

Contract Reports are produced to record the results of scientific work carried out for sponsors, under contract. The ISVR treats these reports as confidential to sponsors and does not make them available for general circulation. Individual sponsors may, however, authorize subsequent release of the material.

UNIVERSITY OF SOUTHAMPTON

INSTITUTE OF SOUND AND VIBRATION RESEARCH

DYNAMICS GROUP

Wheel/Rail Non-Linear Interaction with Coupling between Vertical and Lateral Directions

by

T.X. Wu and D.J. Thompson

ISVR Technical Memorandum No: 891

August 2002

Authorised for issue by
Dr M.J. Brennan
Group Chairman

ABSTRACT

A theoretical model is developed to explore the wheel/rail interaction with coupling between the vertical and lateral directions. This coupling is introduced through the track dynamics due to the offset of the wheel/rail contact point from the rail centre line. Equivalent models of the railway track in the time domain are developed according to the rail vibration receptances in the frequency domain. The wheel is represented by a mass in each direction with no vertical-lateral coupling. The vertical wheel/rail interaction is generated through a non-linear Hertzian contact stiffness, allowing for the possibility of loss of contact between the wheel and rail. The lateral interaction is represented by a contact spring and a creep force damper in series and their values depend on the vertical contact force. The vibration source is the roughness on the wheel and rail contact surfaces which forms a relative displacement excitation in the vertical direction. Using the combined interaction model with this relative displacement excitation, the wheel/rail interactions with coupling between the vertical and lateral vibrations are simulated. It is found that the lateral interaction force caused by the offset is usually less than thirty percent of the vertical dynamic force. The lateral vibration of the rail is significantly reduced due to the presence of the lateral coupling, whereas the vertical interaction is almost unaffected by the lateral force.

CONTENTS

1. INTRODUCTION

Small-scale unevenness on the wheel and rail contact surfaces, referred to as roughness, induces high frequency dynamic interaction between the wheel and rail when a train runs on the track. As a result, the wheel and rail are excited, vibrate and radiate noise. It is important to know the wheel/rail interaction force in order to predict track and wheel vibration, railway noise radiation as well as the formation of rail and wheel corrugation.

Wheel/rail interaction has been studied over many years from different aspects and for different purposes. A review of models for wheel/rail interaction was presented by Knothe and Grassie [1]. Two main kinds of model have been used to study wheel/rail interaction, a moving irregularity between a stationary wheel and rail, and a wheel rolling over irregularities on the track. The moving irregularity model is based on the fact that the structural wave speed in the rail is much higher than train speed in the audio frequency range. Wheel/rail interaction can be studied in either the frequency domain or the time domain. The frequency-domain model was used by Remington [2] and Thompson [3] for studying rolling noise generation, and by Grassie et al. [4] for investigating the formation of short pitch corrugation on the rail head. As the analysis in the frequency domain is only suitable for linear systems, the non-linear characteristics of wheel/rail interaction such as the Hertzian contact force and loss of contact between the wheel and rail cannot be included using a frequency-domain model. A time-domain model can be used to study non-linear interaction between the wheel and rail. Newton and Clark [5] calculated the wheel/rail interaction forces caused by wheel flats using a time-domain model in which the linear wheel/vehicle and track models interact through a non-linear contact stiffness. Andersson and Dahlberg [6] studied the wheel/rail impacts at a railway turnout using a finite element model for the track with a moving vehicle. For a wheel/rail interaction model in the time domain, the track usually is difficult to tackle because it could be infinite and is supported by rail pads, sleepers and ballast. However, if it is assumed to be linear, the track model can be simplified using some techniques. Nielson and Igeland [7] developed a moving wheel/rail interaction model using a method of modal superposition to simplify the track model. A low order multiple degree-of-freedom system was developed by Wu and Thompson [8] to approximate the infinite track and this has been used for calculating wheel/rail impact noise generation [9].

In all the above time-domain models only vertical dynamics are considered. In practice the wheel/rail contact position is often offset a small distance from the rail centre line. The

contact force therefore applies a torsional moment to the rail, causing both lateral and torsional vibration of the rail. As the vibration behaviour of the wheel and rail are different, a relative motion and interaction force in the lateral direction arise between the wheel and rail. The wheel/rail interactions with coupling between vertical and lateral directions have been studied by Thompson [3, 10] using a frequency-domain model. In this linear model, the vertical contact force was assumed to depend linearly on the deflection and no loss of contact was allowed between the wheel and rail. The coupling in the contact area was considered in three co-ordinate directions and three rotational directions. As, in practice, loss of contact may often occur between the wheel and rail when a train runs over corrugated rails or at rail joints, point and crossings, a time-domain model is needed to allow for the non-linear wheel/rail interactions [8, 9].

In this paper a theoretical model is developed to explore the wheel/rail interactions allowing for coupling between the vertical and lateral vibration. Equivalent time-domain models of the railway track are developed according to the rail vibration receptances in the frequency domain in both vertical and lateral directions at the contact point with the wheel. Coupling between lateral and vertical directions is introduced by the offset of the wheel/rail contact point from the rail centre line. The wheel is represented by a mass in each direction with no coupling between vertical and lateral directions. In the vertical direction the wheel and rail interact through a non-linear Hertzian contact stiffness and allowance is made for the possibility of loss of contact between the wheel and rail. The lateral wheel/rail interaction is represented by a contact spring and a creep force damper in series and their values depend on the vertical contact force. The vibration source is the roughness on the wheel and rail contact surfaces which forms a relative displacement excitation in the vertical direction (moving irregularity between a stationary wheel and rail). Using the combined interaction model with the relative displacement excitation, the wheel/rail interactions including coupling between the vertical and lateral vibrations are simulated in the time domain. This study shows that the lateral interaction force caused by the offset is usually less than thirty percent of the vertical dynamic force. The lateral vibration of the rail is significantly reduced by the presence of the lateral force, whereas the vertical interaction is almost unaffected by the lateral force.

2. RAIL RECEPTANCES AT THE WHEEL CONTACT POINT

The track models here are assumed to be linear, although the foundation components such as the rail pad and ballast are actually non-linear with a stiffness varying with the preload applied to them. For a linear system, its analysis can be performed in the frequency domain based on the superposition principle. Moreover, for a linear system calculations can be performed by replacing the system by another linear system having the same frequency response function, even though they are physically different. This provides a useful approach as a complicated physical system such as a track can be replaced by an equivalent system which has a similar frequency response function but is much simpler and easier to tackle mathematically.

The purpose of this section is to introduce the vibration receptances (displacement per unit force) of a track at the wheel contact point which are required for modelling of wheel/rail interactions. According to the track receptances the full track model will be replaced by a mathematically equivalent but simplified model later on in section 3.

Figure 1 shows schematically the track models for both vertical and lateral dynamics. In both cases, the track is approximated by an equivalent continuously supported track. This, therefore, neglects the effects of support periodicity. In the vertical direction the track is described by an infinite Timoshenko beam with continuous spring-mass-spring supports representing rail pad, sleeper and ballast. In the lateral direction the rail vibration behaviour is much more complicated compared with the vertical vibration, because the cross-sectional deformation at high frequencies should be taken into account. A suitable model for lateral vibration of a track was developed by Wu and Thompson [11]. The essential cross-sectional deformation types are rail head bending and torsion, rail foot bending and torsion and the relative motion between the rail head and foot, web bending. A model for lateral vibration of a rail in the frequency range up to 5 kHz should allow all these kinds of deformation. The cross-section of a multiple beam model for lateral vibration is shown in Figure 1(b). In this model the rail is divided into three parts: the head and foot are represented by two infinite Timoshenko beams which can be subjected to both bending and torsion, and the web is replaced by numerous beams along the rail which connect the head and foot. In this simplified model the twisting stiffness and the bending stiffness of the web in the direction of the rail axis vanish. The effects of the web twisting stiffness can be compensated by adjusting the head and foot torsional stiffness. Ignoring the bending stiffness of the web in the rail axis direction will cause no problem because it is much smaller than the lateral bending stiffness of

the rail head and foot. The rail is assumed to be continuously supported by spring-mass-spring layers as for the vertical vibration model. However, the rotational inertia of the sleeper and the rotational stiffness of the ballast are not taken into account, because they are much larger than the rotational inertia of the rail cross-section and the rotational stiffness of the pad respectively, and thus can be approximated as a fixed foundation.

Figures 2-5 show the rail receptances for vertical and lateral vibrations calculated using these models. The dotted lines are the results from the mathematically equivalent models which will be discussed later on in section 3. The corresponding track parameters are listed in Table 1. For vertical vibration the rail receptance α_v is quite simple. Two resonance peaks can be seen, at about 80 Hz and 550 Hz. At 80 Hz the whole track bounces on the vertical stiffness of the ballast, while at 550 Hz the rail vibrates on the pad stiffness.

The lateral vibration of the rail head is coupled with the torsional vibration. This means that a lateral force on the rail head can cause both lateral and torsional vibrations and a torsional moment on the rail head can also cause both. Four receptances α at the rail head centre are therefore needed to describe the lateral dynamics, α_{ll}, α_{lt}, α_{tl} and α_{tt}, where the subscript ij indicates that the displacement i is caused by force j. l and t represent the lateral force or displacement and the torsional moment or rotation respectively. According to the reciprocity principle for linear structures, α_{lt} and α_{tl} are identical.

The translational receptance of the rail head centre α_{ll} is shown in Figure 3. Three well-damped resonances can be seen at about 100 Hz, 160 Hz and 380 Hz. At 100 Hz the whole track bounces on the lateral stiffness of the ballast, but this resonance is highly damped and difficult to observe. At 160 Hz the rail vibrates laterally on the stiffness of the pad. These two resonances correspond to cut-on frequencies of lateral bending waves. At 380 Hz the rail rotates on the pad rotational stiffness and this can be identified as the cut-on of the torsional wave. The other two peaks at about 1400 Hz and 3600 Hz can be identified as the cut-on of the first and second web bending waves respectively, though the latter is not strongly excited. Figure 4 shows the torsional receptance of the rail head α_{tt} which is the rotation of the rail head per unit torque. It can be seen from Figure 4 that the three resonances at 380 Hz, 1400 Hz and 3600 Hz are much stronger because they are more readily excited by a torsional moment. The cross receptance between the translational and torsional vibration α_{lt} is shown in Figure 5. The cross receptance shows features somewhat between the lateral and torsional receptances, apart from the sharp trough at about 3900 Hz. Compared with the vertical

receptance, the lateral receptance of a track is much higher because the pad stiffness is much lower in the lateral direction, the rail bending stiffness is lower, and torsional motion increases the flexibility.

3. EQUIVALENT TRACK MODELS IN THE TIME DOMAIN

A non-linear wheel/rail interaction model in the time domain is required to take account of the Hertzian contact force and allow for the possibility of loss of contact between the wheel and rail. As the track models are assumed to be linear, they can be transformed from the frequency domain to the time domain, according to the rail receptances at the wheel contact point, which are required for modelling of wheel/rail interaction.

Before performing the transformation, it is of considerable benefit to approximate the rail receptance using a transfer function in the form of a ratio of two polynomials, so that conventional system theory can be applied for setting up a mathematical model for the track dynamics in the time domain. The function 'invfreqs' in the Signal Processing Toolbox of MATLAB is used for this task [12]. This function returns the real numerator and denominator coefficient vectors b and a of the transfer function

$$H(s)=\frac{B(s)}{A(s)}=\frac{b_1 s^m+b_2 s^{m-1}+\ldots+b_m s+b_{m+1}}{s^n+a_1 s^{n-1}+\ldots+a_{n-1} s+a_n}, \tag{1}$$

whose complex frequency response approximates the required response, in this case the rail receptance, at specified frequency points. Scalars m and n specify the desired orders of the numerator and denominator polynomials. More details about the algorithm of this function can be found using the Help browser via MATLAB's Help menu. The most important point for using this function is that whatever values of m and n are selected, it must be ensured that all the poles of the returned transfer function $H(s)$ are in the left half-plane and thus the system is stable.

For the four rail receptances in vertical and lateral directions, α_v, α_{ll}, α_{tt} and α_{lt}, four corresponding transfer functions, H_v, H_{ll}, H_{tt} and H_{lt}, based on equation (1) are required to approximate them in the frequency region considered. In Figures 2-5 the frequency responses of these functions are compared with the receptances of the full track model. For the vertical receptance the orders m and n of the transfer function H_v are chosen to be 3 and 4 respectively, whereas for H_{ll} m = 7 and n = 8, for H_{tt} m =13 and n = 14 and for H_{lt} m = 9 and n = 10. It can be seen that the fitted frequency responses of the H functions are in good agreement with the

receptances of the infinite track model in the whole frequency region 50 – 5000 Hz. The values of b_i and a_i for the four transfer functions, H_v, H_{ll}, H_{tt} and H_{lt}, are listed in Table 2. No attempt is made to ensure that the poles of these functions coincide, although from the curve fitting procedure they occur at similar frequencies.

A differential equation corresponding to $H(s)$ in equation (1) can be given

$$(D^n + a_1 D^{n-1} + \ldots + a_{n-1} D + a_n) y(t) = (b_1 D^m + \ldots + b_m D + b_{m+1}) f(t), \tag{2}$$

where D represents the differential operator d/dt. $y(t)$ and $f(t)$ are the output and input of the system and in relation to the track vibration they represent the corresponding rail displacement and wheel/rail interaction force respectively. The state-space representation of equation (2) for the case of $n = m + 1$ can be expressed as follows (see reference [13]):

$$\begin{bmatrix} \dot{x}_1 \\ \dot{x}_2 \\ \vdots \\ \dot{x}_n \end{bmatrix} = \begin{bmatrix} -a_1 & 1 & 0 & \cdots & 0 \\ -a_2 & 0 & 1 & \cdots & 0 \\ \vdots & \vdots & \vdots & & \vdots \\ -a_n & 0 & 0 & \cdots & 0 \end{bmatrix} \begin{bmatrix} x_1 \\ x_2 \\ \vdots \\ x_n \end{bmatrix} + \begin{bmatrix} b_1 \\ b_2 \\ \vdots \\ b_n \end{bmatrix} f(t), \tag{3}$$

$$x_1(t) = y(t). \tag{4}$$

In equation (3) only f and x_1 have explicit physical meanings and represent the force and displacement at the wheel/rail contact point respectively. The other variables have no direct physical meaning. Nevertheless applying the above procedure to the four transfer functions H_v, H_{ll}, H_{tt} and H_{lt}, which approximate the rail receptances α_v, α_{ll}, α_{tt} and α_{lt}, the equations of motion in the time domain can be obtained for an infinite track at the wheel/rail contact point.

4. WHEEL/RAIL INTERACTION MODELLING

The wheel/rail interaction model with coupling between the vertical and lateral vibrations is shown schematically in Figure 6. The main source of coupling considered results from the offset of the wheel/rail contact point from the rail centre line. Due to the presence of the offset δ, the vertical interaction force f_v applies a torsional moment to the rail head, causing both lateral and torsional vibration of the rail. f_v can be quasi-statically determined by using Hertz contact theory. As the vibration of the wheel differs from that of the rail, a relative motion and lateral interaction force arise between the wheel and rail. In addition to the relative motion, the relative elastic deformation between the wheel and rail should also be take into account. The lateral interaction force f_l is therefore assumed to be related to a contact spring and a creep

damper in series. This model for lateral wheel/rail interaction was developed by Thompson [10, 14] in the frequency domain, based on Knothe and Gross-Thebing's work concerning rolling contact at high frequencies [15].

For simplicity the wheel is regarded as a mass in vertical and lateral directions. In the vertical direction the wheel is represented by the unsprung mass M_{wx}, whereas in the lateral direction the wheel mass M_{wy} includes the effect of the rotation about the z axis (z is the direction out of the page in Figure 6). The wheel masses are M_{wx} = 595 kg and M_{wy} = 865 kg. This simplified wheel model neglects the high frequency modes of the wheel. The equations of motion for the mass wheel are given as

$$M_{wx}\ddot{x}_w = W - f_v, \tag{5}$$

$$M_{wy}\ddot{y}_w = -f_l', \tag{6}$$

where W represents the load from the vehicle weight, f_l' is the lateral interaction force acting on the wheel. f_l' is slightly different from f_l, the lateral interaction force acting on the rail, because a small mass m is added between the spring k_T and damper c to avoid mathematical difficulties.

The non-linear Hertzian contact force f_v is given by

$$f_v = C_H (x_w - x_r - r)^{3/2},$$

$$f_v = 0, \quad \text{when } x_w - x_r - r \le 0, \tag{7a, b}$$

where x_w and x_r are the wheel and rail displacement in the vertical direction at the contact point respectively, r is the roughness excitation, effectively moving at the train speed V, C_H is the Hertzian constant, taken here as C_H = 93.7 GN/m$^{3/2}$. The lateral interaction forces are calculated using the following formulae

$$f_l = k_T (y_m - y_r),$$

$$f_l' = c(\dot{y}_w - \dot{y}_m),$$

$$f_l = f_l' = 0, \text{ when } f_v = 0,$$

$$m\ddot{y}_m = f_l' - f_l, \tag{8a-8d}$$

where y_w and y_r are the wheel and rail displacement in the lateral direction at the contact point respectively, y_m is the displacement of the small mass m.

The rail displacements at the wheel contact point, x_r and y_r, can be calculated by

$$x_r = x_{rc} + \delta\theta_r,$$

$$y_r = y_{rc} + h\theta_r/2, \tag{9a, b}$$

where h is the rail head height, x_{rc}, y_{rc} and θ_r are the vertical, lateral and rotational displacement of the rail head centre respectively and can be calculated using the equivalent track models in the time domain, which have been developed in the previous section according to the track receptances. For the lateral and rotational displacements y_{rc} and θ_r, each contains two components, caused by the lateral force f_l and torsional moment f_t respectively. f_t is given as

$$f_t = f_v\delta + f_l\, h/2\,. \tag{10}$$

The lateral contact spring k_T is about 20% stiffer than the vertical contact stiffness [14] and can be determined by

$$k_T = 1.2k_H = 1.8C_H^{2/3} f_v^{1/3}, \tag{11}$$

where k_H represents the equivalent vertical contact stiffness at a load of f_v.

The lateral damper c, which is related to the creep force between the wheel and rail, is given as [14]

$$c = \frac{EabC_{22}}{2(1+\nu)V}, \tag{12}$$

where a and b are the semi-axes of the contact patch, E and ν are the Young's modulus and Poisson's ratio respectively, the wheel and rail materials being assumed identical, C_{22} is the lateral creepage coefficient and V is the wheel rolling speed. Assuming $a \approx b$, $\nu = 0.3$ and thus C_{22} = 3.7 [16], for the wheel radius r_w = 0.46 m the damper c can be estimated using the following simplified formula

$$c \approx \frac{E^{1/3} f_v^{2/3}}{V}. \tag{13}$$

5. SIMULATION OF WHEEL/RAIL INTERACTIONS

Numerical simulations are carried out using the models introduced in the previous sections for the wheel/rail interactions with coupling between the vertical and lateral directions due to the offset of the contact position. The offset is assumed to be constant, although it varies in practice and could be on either side of the rail centre line. The excitation is the roughness on the rail and wheel contact surfaces. When a train runs on the rails, the roughness forms an excitation with multiple frequency components which can be regarded as a broad band random process.

Figure 7 shows a typical 1/3 octave band roughness spectrum. This spectrum corresponds to the roughness of a wheel with cast-iron block brakes on corrugated rail at 140 km/h [17]. Starting from this spectrum, a narrow-band spectrum is generated with a bandwidth of 5 Hz, which corresponds to the 1/3 octave band spectrum. Below 50 Hz the magnitude of the spectrum is set to zero. This narrow-band spectrum is then used to generate a time series by using the inverse Fourier transform, the phase of each Fourier component being chosen randomly between $-\pi$ and π. This time series is used as the roughness input to the wheel/rail system.

The fourth order Runge-Kutta method is used for the numerical simulations. Two sets of offset and vehicle load are used in the calculations. These are $\delta = 10$ and 30 mm, $W = 50$ and 100 kN. The wheel rolling speed is chosen to be $V = 140$ km/h, corresponding to the roughness spectrum. The results are shown in terms of the interaction forces and dynamic displacements of the wheel and rail in the vertical and lateral directions. For a better resolution they are shown only within a period of 0.05 second, although the simulations are carried out for about 0.11 second.

Figures 8 and 9 show the results for an offset $\delta = 10$ and 30 mm respectively, under a static load $W = 100$ kN. The variation in the vertical interaction force can be seen to be quite large. A sharp peak of the interaction force appears when a sharp negative roughness input is applied, which according to the sign convention adopted corresponds to an asperity. Loss of contact occurs just after 0.025 second in the case of 10 mm offset (Figure 8), where there is a large asperity in the roughness, so that the interaction forces vanish. The wheel and rail displacements generally follow the roughness input, although the wheel cannot follow the high frequency components of the input due to its large inertia and thus responds as a low pass filter. It can be observed from the phase of the rail vibration that when a dip occurs in the roughness, the rail bounces upwards, whereas an asperity squeezes the rail downwards, as would be expected. The vertical interaction force for the 30 mm offset can be seen to fluctuate considerably less than that for the 10 mm offset. This results from the fact that an additional displacement of the rail in the vertical direction can arise due to the rotation of the rail head caused by the torsional moment which is related to the offset. Thus the vertical stiffness of the rail/track at the wheel contact point is smaller for the 30 mm offset than for the 10 mm offset.

The lateral interaction force is found to be much smaller than the vertical dynamic force. It is generated because the lateral vibration of the wheel and rail are different and a relative motion arises between them. As a larger offset causes a larger relative motion in the lateral

direction, the interaction force due to 30 mm offset is about three times as large as that due to 10 mm offset. Moreover it can be observed that the dominant frequency in the lateral interaction force and rail displacement is close to the cut-on frequency of the first order web bending of the rail, which is about 1400 Hz. When loss of contact occurs, the rail can be seen to move considerably relative to the wheel in the lateral direction.

An interesting phenomenon is that the wheel can be seen to move relative to the rail, always in the positive direction due to the creepage between the wheel and rail. This is because the creep force between the wheel and rail is not symmetric. When an asperity in the roughness occurs, the rail head is squeezed down and rotates clockwise due to the offset assumed, see Figure 6. The rail head therefore moves laterally in the positive direction and tends to slide over the wheel at the contact point as the wheel cannot immediately follow the rail due to its inertia. Thus a creep force is generated in the wheel/rail contact area to push the wheel in the positive direction. When a dip occurs in the roughness, the rail head bounces back and rotates anti-clockwise, and thus applies a creep force to the wheel to push it in the negative direction. However, the creep forces in the two situations are different. The creep force corresponding to an asperity (in the positive direction to the wheel) is larger than that corresponding to a dip (in the negative direction to the wheel). This is because an asperity increases the vertical contact force and a dip decreases it. The damper rate c in equation (8b) increases with the vertical contact force, see equation (13). As a result, a larger damper rate generates a larger creep force for the same relative speed between the wheel and rail. As the creep force on the wheel is always larger in the positive direction than in the negative direction, the wheel has a tendency to move away from the rail in the positive direction. In practice, however, the offset of the wheel/rail contact point from the rail centre line varies and can be on either side of the rail. Moreover lateral creep forces act on both wheels of a wheelset. Thus the wheel position in fact oscillates about a stable position and will not move laterally relative to the rail indefinitely.

Figure 10 shows the results from a 10 mm offset but with only a 50 kN static load applied to the wheel. The roughness input here is the same as before. Compared with the results from the 100 kN static load, more loss of contact occurs between the wheel and rail, as it is more difficult for the 50 kN static load to maintain the wheel and rail in contact under the same roughness input. Many impacts can be observed in Figure 10 in the lateral wheel/rail interaction. These occur following each loss of contact. This is because, when the wheel

contacts the rail again after loss of contact, the difference between the wheel and rail velocities may cause a rapid increase in the interaction force.

The one-third octave band spectra of the wheel/rail interaction forces are shown in Figure 11, corresponding to the time series shown in Figures 8 and 9, where the static load is 100 kN and the offset is 10 and 30 mm. In the vertical force spectra the peaks between 200-250 Hz match the trough in the rail receptance at about 250 Hz, see Figure 2, whereas the peaks around 900 Hz correspond to the peak in the roughness spectrum in Figure 7. The lateral force spectra show a high level around the 1250 Hz band. This corresponds to the first order web bending of the rail at 1400 Hz, see Figure 4. The rail web bending therefore plays an important role in the lateral interaction of the wheel and rail caused by the offset.

Comparing the vertical and lateral interaction force spectra, the vertical force is greater by about 25 dB below 1 kHz and by 12-15 dB above 1.3 kHz when the offset is 10 mm. However, when the offset becomes 30 mm, the lateral force increases and the vertical force decreases, with the differences being 15-20 dB at low frequencies and only 4-8 dB at high frequencies. Also in Figure 11, one-third octave band spectra of the wheel and rail vibration are given. These show similar trends, although the difference between the vertical and lateral response spectra is less than the corresponding difference between the force spectra. This is because the receptance of the lateral vibration of the rail is greater than that of the vertical vibration.

To examine the effects on the vertical interaction of the lateral interaction between the wheel and rail, a situation is simulated, in which the lateral interaction force is set to zero, although a 30 mm offset is assigned. The result from this case is shown in Figure 12 in terms of the lateral displacement of the rail—the interaction force and wheel displacement in the lateral direction are zero. The lateral displacement can be seen to be dramatically larger than that in Figure 9 where the lateral interaction force is non-zero. The vertical interaction force, wheel and rail displacements are not shown because in the absence of lateral interaction, the vertical interaction between the wheel and rail is almost unaffected. The vertical force decreases slightly and the vertical displacements of the wheel and rail increase slightly.

6. CONCLUSIONS

The wheel/rail non-linear dynamic interactions have been studied with coupling between the vertical and lateral directions due to the offset of the wheel/rail contact position from the rail

centre line. A theoretical model for the wheel/rail interaction in the time domain is developed in which the equivalent models of the railway track are developed according to the rail vibration receptances in the frequency domain at the contact point with the wheel. In this model the wheel and rail interact through a non-linear Hertzian contact stiffness in the vertical direction, a contact spring and a creep force damper in series in the lateral direction, and the possibility of loss of contact between the wheel and rail is taken into account. Using this model the wheel/rail interactions with coupling between the vertical and lateral vibrations are simulated under a broad band relative displacement excitation.

Lateral wheel/rail interaction under a vertical roughness excitation arises because of the offset of the wheel/rail contact point from the rail centre line. It is found that the lateral interaction force between the wheel and rail depends on the offset values. The lateral force increases with the offset, as does the rail displacement in lateral direction. Within an offset range 10-30 mm, which usually occurs in practice, the lateral interaction force is generally less than thirty percent of the vertical dynamic force in terms of the peak values. On the other hand, the vertical interaction force decreases with increasing offset because the vertical stiffness of the track at the wheel contact point reduces. The lateral wheel/rail interaction is generated through the rotation of the rail head, and thus the lateral force and displacement of the rail have large components around the cut-on frequency of the first order web bending of the rail. Although the lateral interaction force between the wheel and rail is smaller than the vertical dynamic force, the difference between them is only a few dB at high frequencies when the offset is large. The presence of the lateral interaction significantly reduces the rail vibration in the lateral direction, because it always resists the relative motion between the wheel and rail. However the vertical interaction is almost unaffected by the inclusion of the lateral interaction force.

Although the offset is assumed to be fixed in this study, if it can be estimated using vehicle dynamics simulations [18, 19], the rail vibration in the lateral direction could be predicted under the roughness excitation after the lateral interaction force has been calculated using the approach in this study. Finally, it should be pointed out that the wheel has been treated as a concentrated mass in this study. If its modal behaviour is included, this will also provide a source of coupling between the vertical and lateral directions and can be expected to affect the magnitude of the lateral force.

7. ACKNOWLEDGEMENTS

The work described has been performed within the project 'Non-linear Effects at the Wheel/rail Interface and their Influence on Noise Generation' funded by EPSRC (Engineering and Physical Sciences Research Council of the United Kingdom), grant GR/M82455.

REFERENCES

1. K. Knothe and S. L. Grassie 1993 *Vehicle System Dynamics* 22, 209-262. Modelling of railway track and vehicle/track interaction at high frequencies.
2. P. J. Remington 1987 *J. Acoust. Soc. Am.* 81, 1805-1823. Wheel/rail rolling noise I: theoretical analysis.
3. D. J. Thompson 1993 *Journal of Sound and Vibration* 161, 387-400. Wheel-rail noise generation, part I: introduction and interaction model.
4. S. L. Grassie, R. W. Gregory, D. Harrison and K. L. Johnson 1982 *Journal Mechanical Engineering Science* 24, 77-90. The dynamic response of railway track to high frequency vertical excitation.
5. S. G. Newton and R. A. Clark 1979 *Journal Mechanical Engineering Science* 21, 287-297. An investigation into the dynamic effects on the track of wheelflats on railway vehicles.
6. C. Andersson and T. Dahlberg 1998 *Proceedings of the Institution of Mechanical Engineers Part F* 212, 123-134. Wheel/rail impacts at a railway turnout crossing.
7. J. C. O. Nielson and A. Igeland 1995 *Journal of Sound and Vibration* 187, 825-839. Vertical dynamic interaction between train and track—influence of wheel and track imperfections.
8. T. X. Wu and D. J. Thompson 2000 *Vehicle System Dynamics* 34, 261-282. Theoretical investigation of wheel/rail non-linear interaction due to roughness excitation.
9. T. X. Wu and D. J. Thompson 2002 *Journal of Sound and Vibration* 251, 115-139. A hybrid model for the noise generation due to railway wheel flats.
10. D. J. Thompson 1993 *Journal of Sound and Vibration* 161, 447-466. Wheel-rail noise generation, part IV: contact zone and results.
11. T. X. Wu and D .J. Thompson 1999 *J. Acoust. Soc. Am.* 106, 1369-1376. Analysis of lateral vibration behaviour of railway track at high frequencies using a continuously supported multiple beam model.
12. MATLAB, The MathWorks Inc., version 5.3.1, 1999.
13. F. H. Raven 1978 *Automatic Control Engineering*. Tokyo: McGraw-Hill; third edition.
14. D. J. Thompson 1990 *Ph.D. Thesis, University of Southampton*. Wheel-rail noise: theoretical modelling of the generation of vibrations.

15. K. Knothe and A. Gross-Thebing 1986 *Vehicle System Dynamics* 15, 133-153. Derivation of frequency dependent creep coefficients based on an elastic half-space model.
16. J. J. Kalker 1990 *Three-dimensional elastic bodies in rolling contact*. Dordrecht: Kluwer Academic Publishers.
17. P. C. Dings, M. G. Dittrich 1996 *Journal of Sound and Vibration* 193, 103-112. Roughness on Dutch railway wheels and rails.
18. A. O. Gilchrist 1998 *Proceedings of the Institution of Mechanical Engineers Part F* **212**(F3), 219-226. The long road to solution of the railway hunting and curving problems.
19. Iwnicki S. (ed) 1999 *Vehicle System Dynamics Supplement* The Manchester Benchmarks for Rail Vehicle Simulation, Swets & Zeitlinger B.V. Lisse 1999.

Table 1. Track parameters

Young's modulus of rail, N/m^2	E	2.1×10^{11}
Shear modulus of rail, N/m^2	G	0.77×10^{11}
Density of rail, kg/m^3	ρ	7850
Loss factor of rail	η_r	0.01
Cross-sectional area of rail (vertical vibration), m^2	A	7.65×10^{-3}
Area moment of inertia, m^4	I	30.6×10^{-6}
Shear coefficient	κ	0.4
Cross-sectional area of rail head (lateral vibration), m^2	A_h	2.85×10^{-3}
Head area moment of inertia, m^4	I_h	1.26×10^{-6}
Head polar moment of inertia, m^4	I_{hp}	1.63×10^{-6}
Head torsional moment of inertia, m^4	J_h	1.03×10^{-6}
Cross-sectional area of rail foot, m^2	A_f	2.63×10^{-3}
Foot area moment of inertia, m^4	I_f	4.92×10^{-6}
Foot polar moment of inertia, m^4	I_{fp}	4.99×10^{-6}
Foot torsional moment of inertia, m^4	I_{fp}	0.40×10^{-6}
Cross-sectional area of rail web, m^2	A_w	2.17×10^{-3}
Web area moment of inertia, m^4	I_w	0.63×10^{-6}
Shear coefficient	κ_l	0.85
Pad vertical stiffness, N/m^2	k_{pv}	583×10^6
Pad lateral stiffness, N/m^2	k_{pl}	83×10^6
Pad rotational stiffness, N/m	k_{pr}	1.09×10^6
Pad loss factor	η_p	0.25
Sleeper mass, kg/m	m_s	270
Ballast vertical stiffness, N/m^2	k_{bv}	83×10^6
Ballast lateral stiffness, N/m^2	k_{bl}	133×10^6
Ballast loss factor	η_b	1.0

Table 2. Parameters of the equivalent track models

	Vertical		
a_1	1.6761×10^{3}	b_1	3.5559×10^{-6}
a_2	1.2297×10^{7}	b_2	1.8468×10^{-2}
a_3	7.2643×10^{9}	b_3	2.4479×10^{1}
a_4	3.6736×10^{12}	b_4	3.9058×10^{4}
	Lateral		
a_1	2.8598×10^{4}	b_1	6.2238×10^{-6}
a_2	4.4224×10^{8}	b_2	3.0342×10^{-1}
a_3	3.4818×10^{12}	b_3	5.5210×10^{3}
a_4	3.0254×10^{16}	b_4	5.3632×10^{7}
a_5	7.6257×10^{19}	b_5	4.3702×10^{11}
a_6	1.6708×10^{23}	b_6	2.1227×10^{15}
a_7	1.5002×10^{26}	b_7	2.6077×10^{18}
a_8	1.1427×10^{29}	b_8	5.5824×10^{21}
	Lateral/torsional cross		
a_1	1.5119×10^{4}	b_1	4.5769×10^{-5}
a_2	9.5497×10^{8}	b_2	9.8267×10^{-1}
a_3	9.9257×10^{12}	b_3	5.7395×10^{4}
a_4	2.4787×10^{17}	b_4	8.2387×10^{8}
a_5	1.1470×10^{21}	b_5	2.0146×10^{13}
a_6	1.5502×10^{25}	b_6	1.4983×10^{17}
a_7	2.7885×10^{28}	b_7	1.2254×10^{21}
a_8	1.0267×10^{32}	b_8	6.0230×10^{24}
a_9	6.6545×10^{34}	b_9	6.8659×10^{27}
a_{10}	8.3890×10^{37}	b_{10}	1.4691×10^{31}
	Torsional		
a_1	4.4406×10^{4}	b_1	1.0180×10^{-2}
a_2	2.4763×10^{9}	b_2	6.2202×10^{2}
a_3	6.8442×10^{13}	b_3	2.3715×10^{7}
a_4	2.0412×10^{18}	b_4	8.6420×10^{11}
a_5	3.6404×10^{22}	b_5	1.6915×10^{16}
a_6	6.9693×10^{26}	b_6	3.9925×10^{20}
a_7	7.6440×10^{30}	b_7	4.6110×10^{24}
a_8	9.3628×10^{34}	b_8	6.9050×10^{28}
a_9	5.2252×10^{38}	b_9	4.3853×10^{32}
a_{10}	4.1943×10^{42}	b_{10}	3.8394×10^{36}
a_{11}	7.5372×10^{45}	b_{11}	1.0007×10^{40}
a_{12}	2.5604×10^{49}	b_{12}	3.7902×10^{43}
a_{13}	1.5991×10^{52}	b_{13}	2.8040×10^{46}
a_{14}	2.1636×10^{55}	b_{14}	4.5029×10^{49}

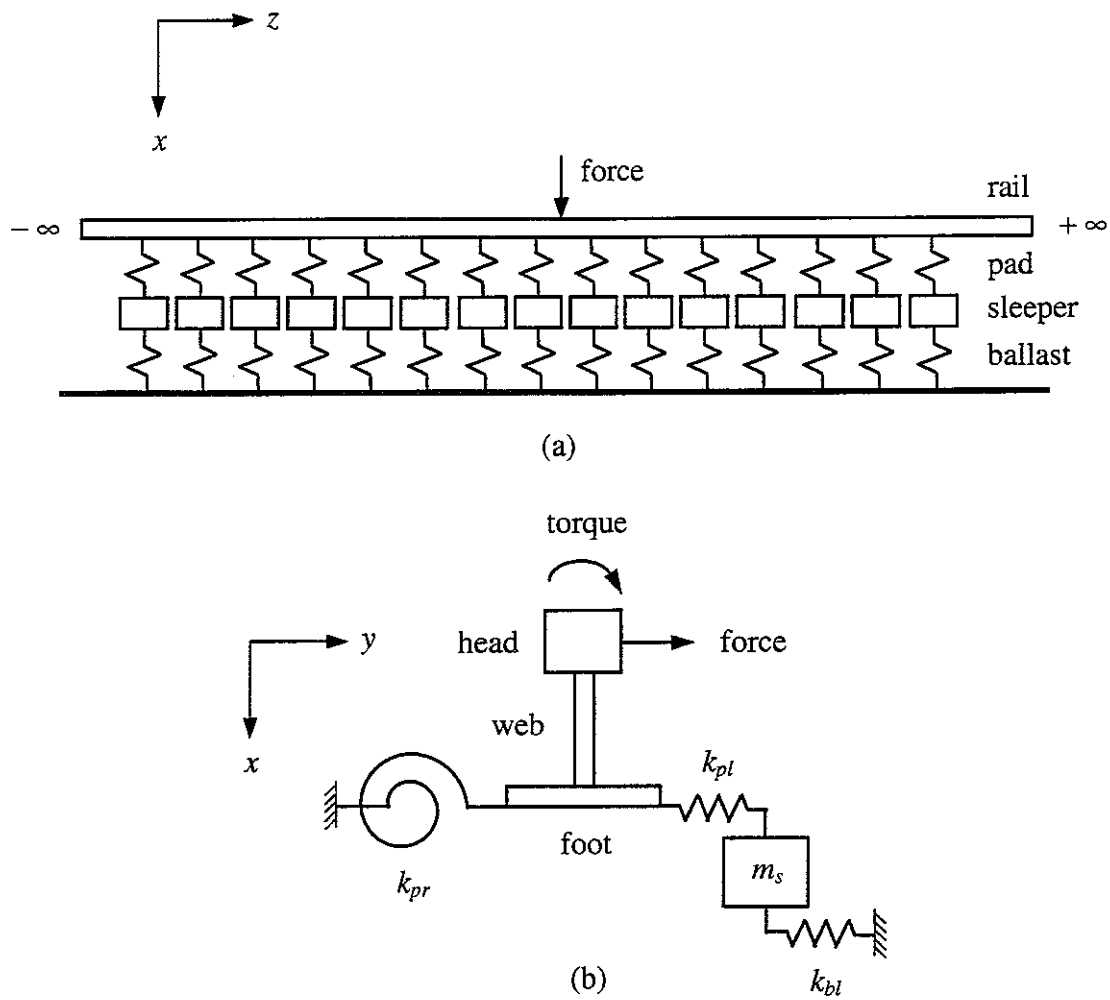

Figure 1. Track dynamics model. (a) for vertical vibration, (b) for lateral vibration.

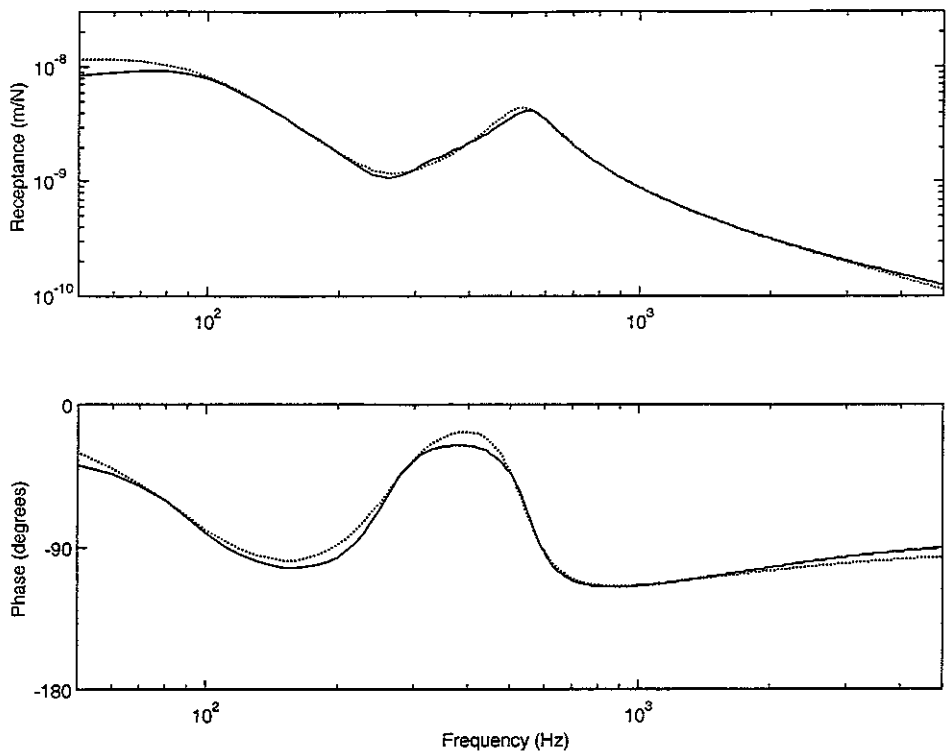

Figure 2. Magnitude and phase of vertical receptance of the rail. —— from full track model, ····· from equivalent model.

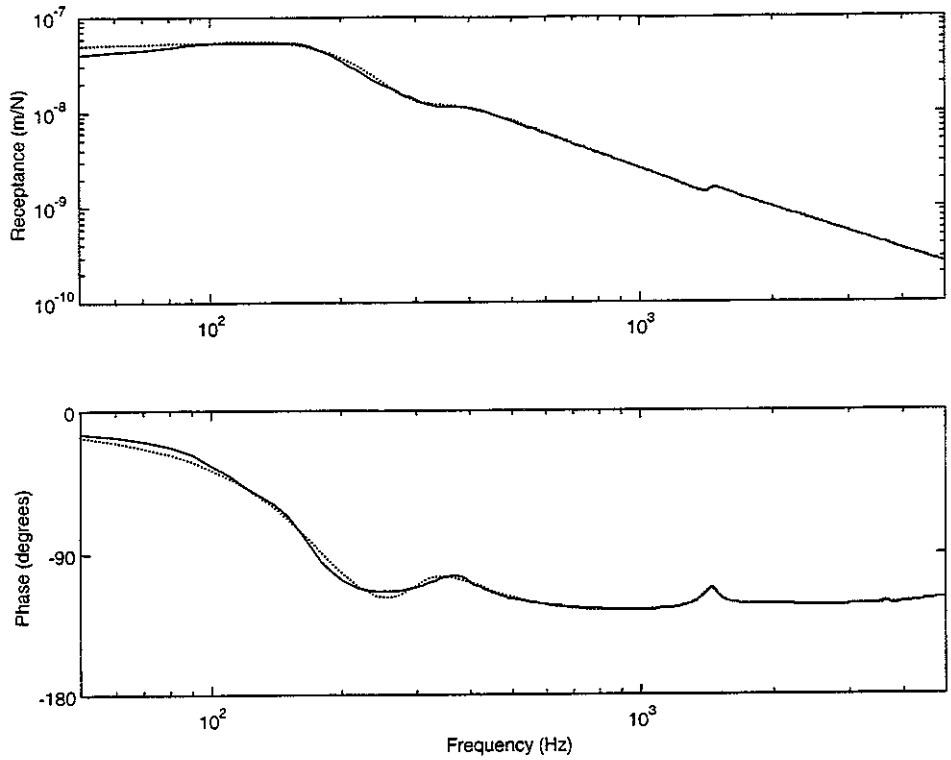

Figure 3. Magnitude and phase of lateral receptance of the rail. —— from full track model, ····· from equivalent model.

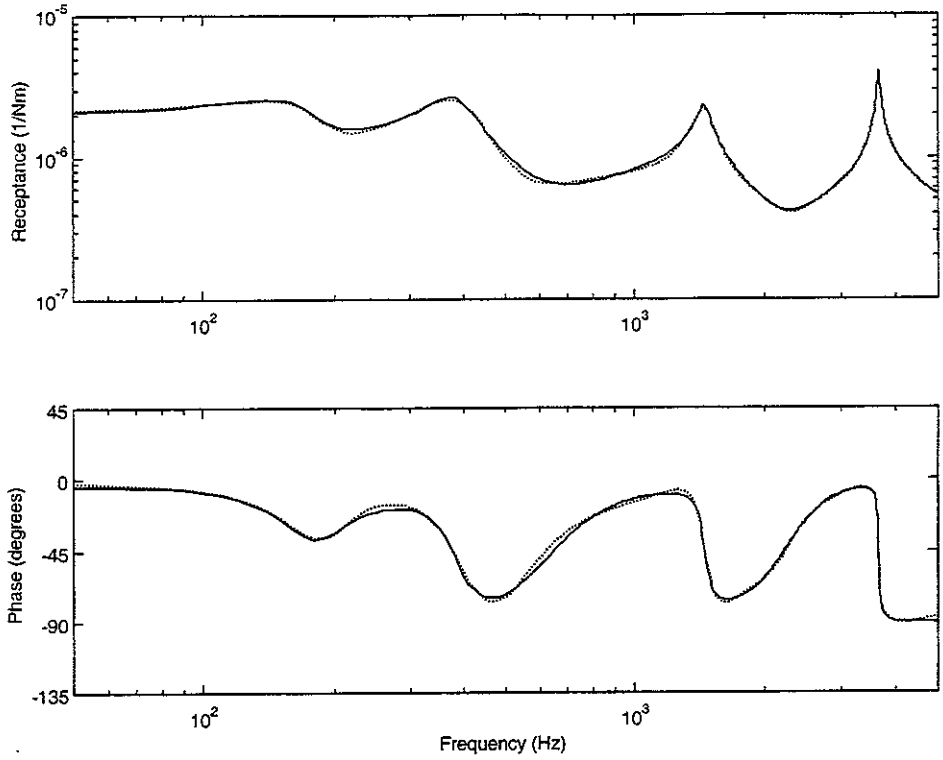

Figure 4. Magnitude and phase of torsional receptance of the rail. —— from full track model, ····· from equivalent model.

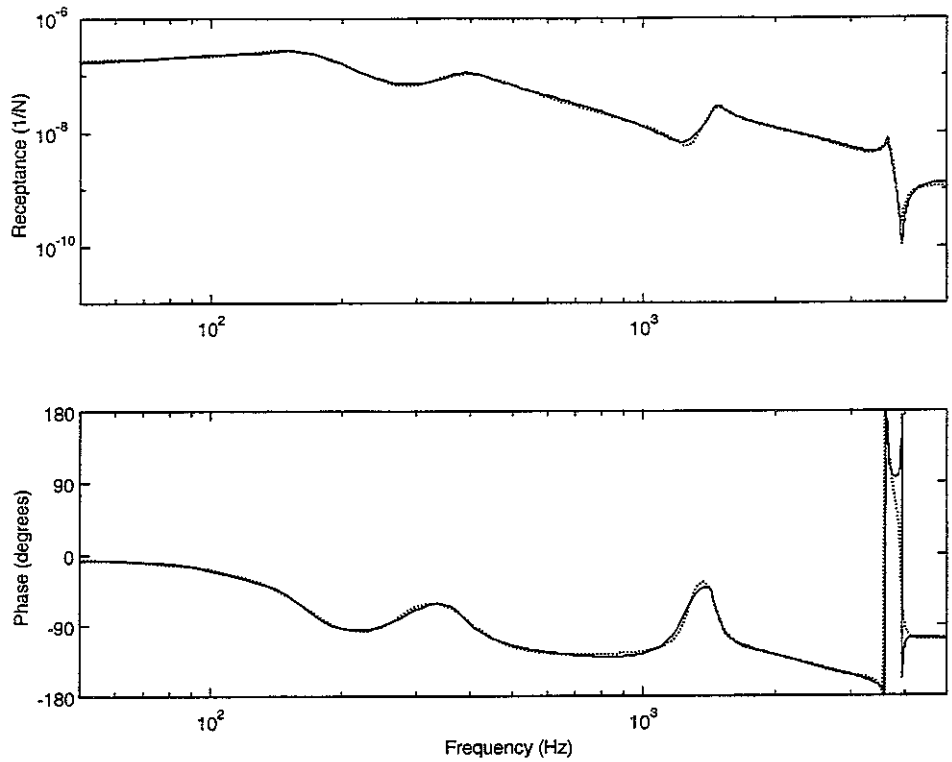

Figure 5. Magnitude and phase of cross receptance of the rail between torsional and translational displacement. —— from full track model, ····· from equivalent model.

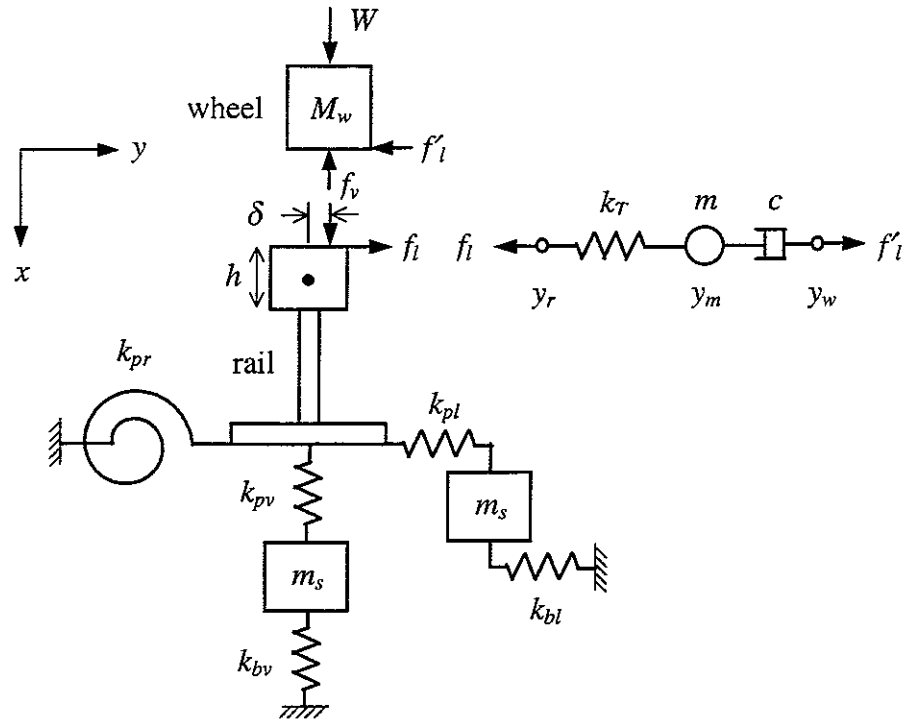

Figure 6. Wheel/rail interaction model with coupling between vertical and lateral vibrations.

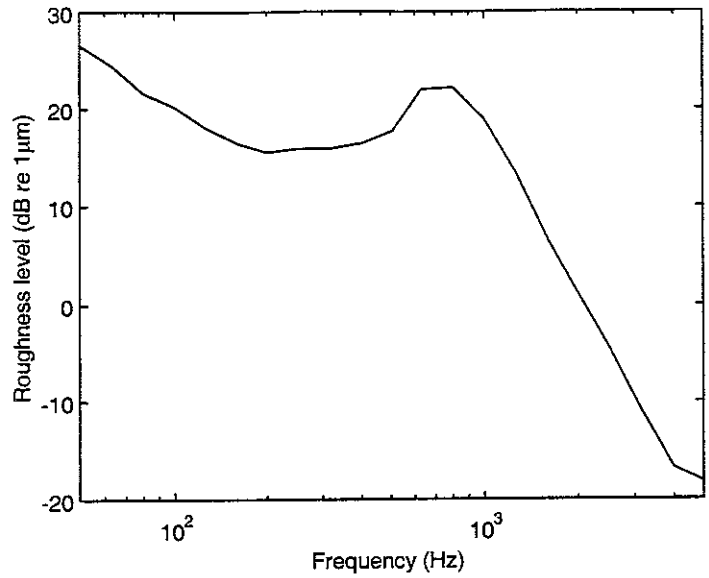

Figure 7. One-third octave band roughness spectrum of corrugated rail at 140 km/h.

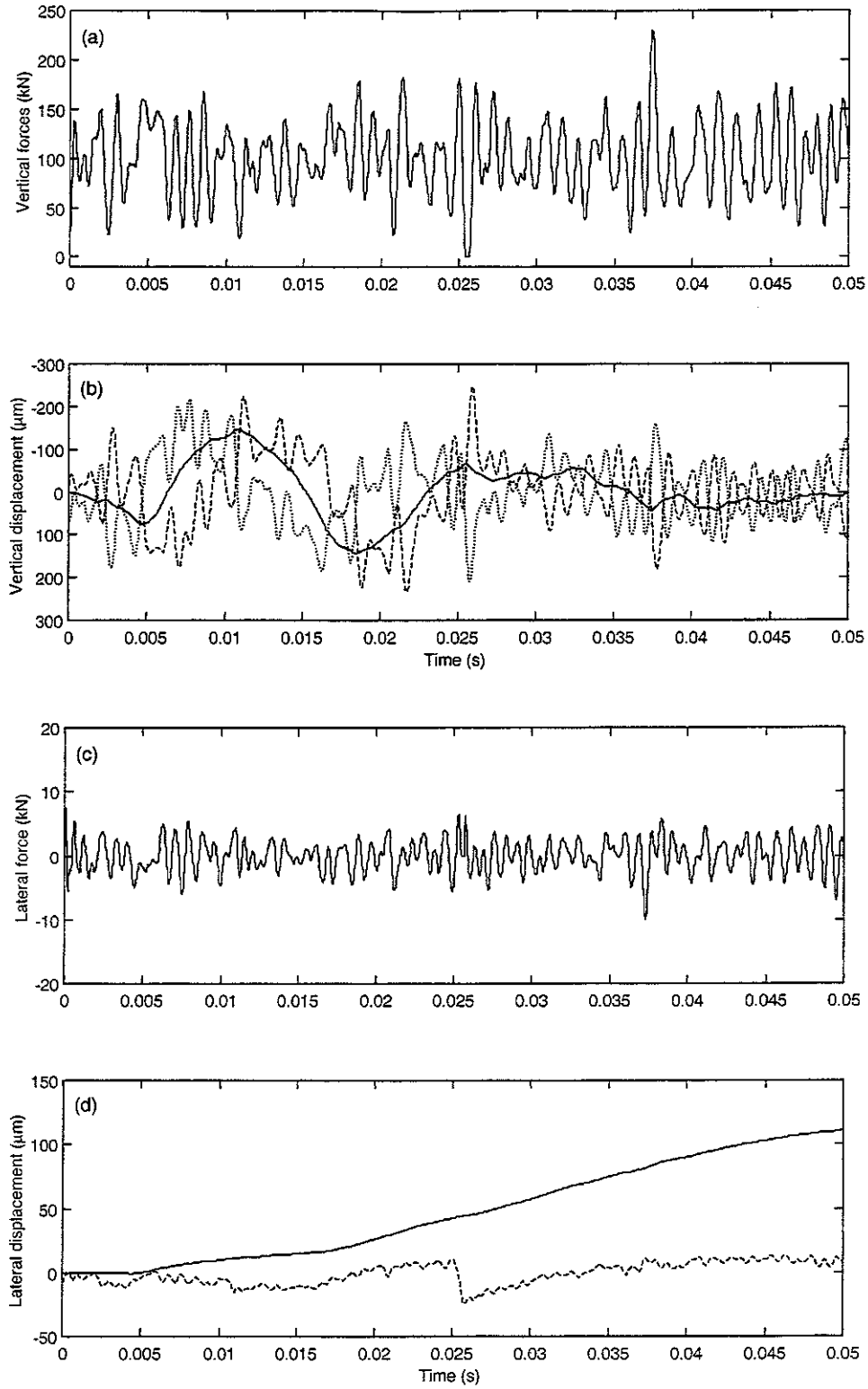

Figure 8. Results for an offset δ = 10 mm and a static load W = 100 kN for a broad-band roughness input from spectrum in Figure 7. (a) Vertical interaction forces, (b) vertical displacements —— wheel, - - - rail, ····· roughness input, (c) Lateral interaction force, (d) vertical displacements —— wheel, - - - rail.

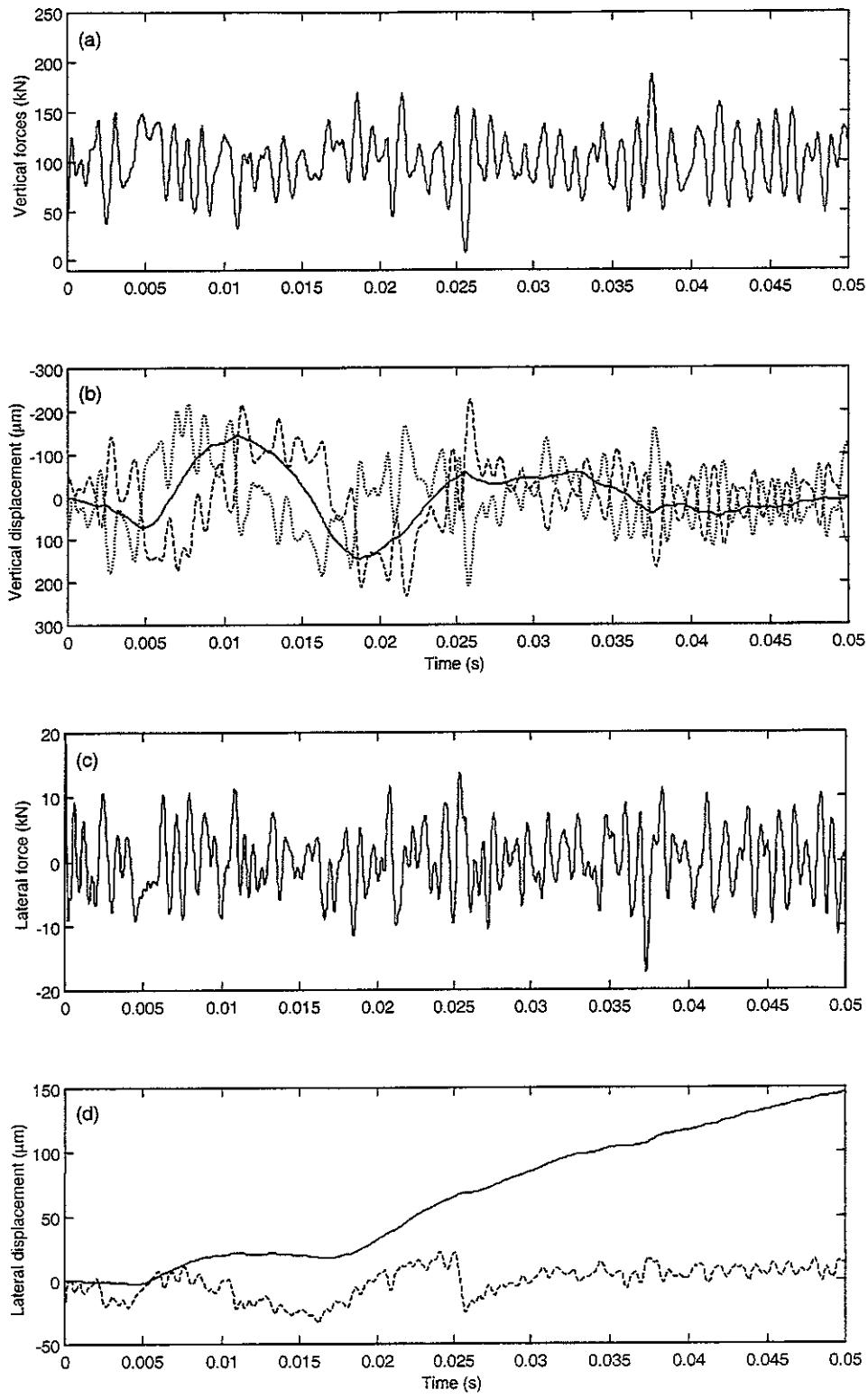

Figure 9. Results for an offset $\delta = 30$ mm and a static load $W = 100$ kN for a broad-band roughness input from spectrum in Figure 7. (a) Vertical interaction forces, (b) vertical displacements —— wheel, - - - rail, ····· roughness input, (c) Lateral interaction force, (d) vertical displacements —— wheel, - - - rail.

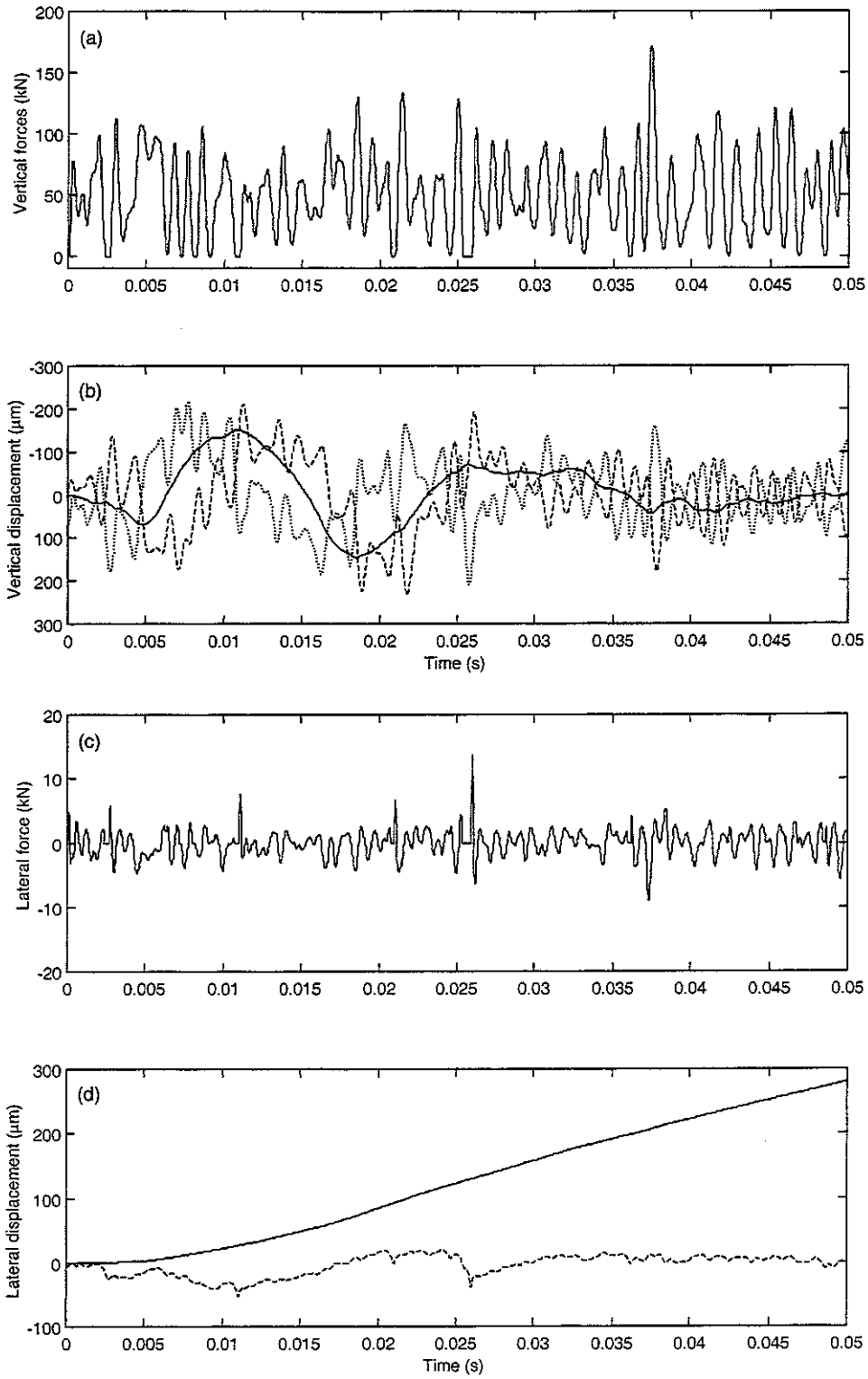

Figure 10. Results for an offset δ = 10 mm and a static load W = 50 kN for a broad-band roughness input from spectrum in Figure 7. (a) Vertical interaction forces, (b) vertical displacements —— wheel, - - - rail, ····· roughness input, (c) Lateral interaction force, (d) vertical displacements —— wheel, - - - rail.

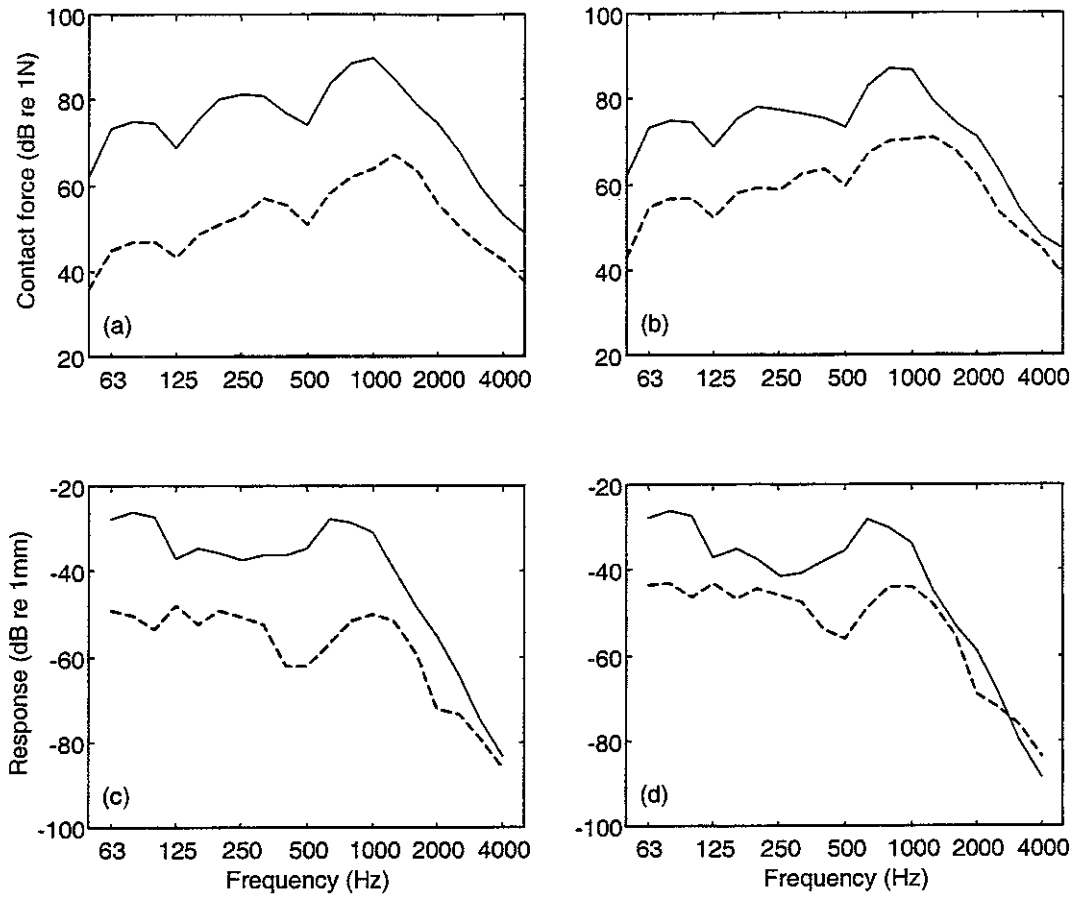

Figure 11. One-third octave band spectra of results corresponding to Figures 8 and 9, with $W = 100$ kN. (a) Wheel/rail interaction forces for $\delta = 10$ mm, (b) wheel/rail interaction forces for $\delta = 30$ mm, (c) displacements for $\delta = 10$ mm, (d) displacements for $\delta = 30$ mm. —— vertical, - - - lateral.

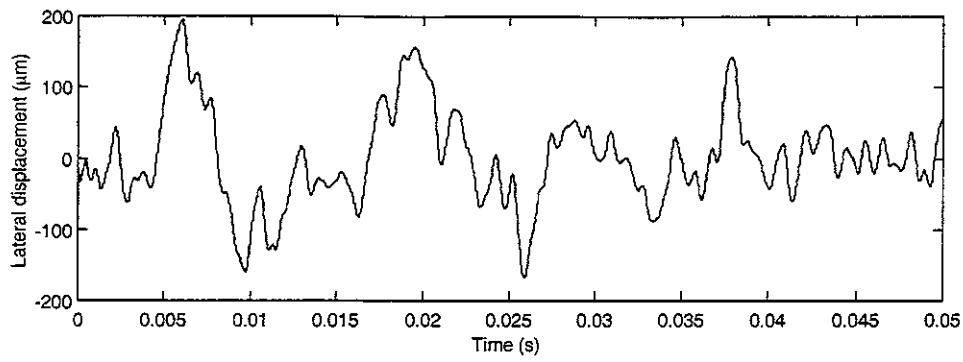

Figure 12. Lateral rail displacement under broad band roughness input as in Figure 9 for a offset δ = 30 mm and a static load to wheel W = 100 kN, but the lateral interaction force is set to zero.